Pakistan Veterinary Journal

ISSN: 0253-8318 (PRINT), 2074-7764 (ONLINE)
DOI: 10.29261/pakvetj/2026.090

RESEARCH ARTICLE

Voltage-dependent anion channel 1(VDAC1)-Mediated Mitophagy: A Potential Therapeutic Target for Mitochondrial Damage Induced by Molybdenum and Cadmium Co-Exposure in Sheep Hepatocytes

He Bai[1,2,†], Lingli Liu[1,†], Chenghong Xing[1], Feiyan Gao[1], Zhou Jiang[1], Yun Wang[1], Zhiwei Xiong[1], Xueyan Dai[1], Fan Yang[1] and Huabin Cao[1*]

[1]Jiangxi Provincial Key Laboratory for Animal Health, Institute of Animal Population Health, College of Animal Science and Technology, Jiangxi Agricultural University, No. 1101 Zhimin Avenue, Economic and Technological Development District, Nanchang 330045, Jiangxi, P. R. China; [2] College of Life Sciences, Mudanjiang Medical University, No. 3 Tongxiang street, Aimin District, Mudanjiang 157011, Heilongjiang, P. R. China. †The first two authors contributed equally to this work.
*Corresponding author: chbin20020804@jxau.edu.cn

ARTICLE HISTORY (25-860)

Received: September 07, 2025
Revised: March 01, 2026
Accepted: March 07, 2026
Published online: April 21, 2026

Key words:
Mitophagy
Molybdenum and Cadmium
Sheep hepatocyte

ABSTRACT

While molybdenum (Mo) is essential for biological processes, overexposure can result in liver failure. Cadmium (Cd) is widely present in the environment, which interferes with the normal metabolic processes within cells. Mitochondria are the main target organ of heavy metal toxicity, and the coping mechanism of mitochondria under Mo and Cd co-exposure is still worthy of further study. This study aimed to decipher the mitochondrial quality control response in sheep hepatocytes under Mo and Cd co-exposure. Using an *In vitro* model, we found that Mo/Cd induced mitochondrial ultrastructural damage, dysfunction (elevated reactive oxygen species (ROS), reduced mitochondrial membrane potential (MMP) and adenosine triphosphate (ATP)), and disrupted dynamics by promoting fission proteins dynamin-related protein 1 (Drp1) and fission 1 (Fis1) while suppressing fusion proteins optic atrophy 1 (OPA1) and mitofusin 2 (Mfn2), thereby triggering excessive mitophagy. Interestingly, inhibiting mitophagy with cyclosporin A (CsA) exacerbated the injury, whereas targeting the mitochondrial porin Voltage-dependent anion channel 1(VDAC1) with VBIT-4 (a small-molecule VDAC1 inhibitor) attenuated both mitophagy and dysfunction. VBIT-4 restored membrane potential, rebalanced dynamics, and improved energy production, indicating that VDAC1-mediated mitophagy acts as a pivotal adaptive mechanism. Our findings propose VDAC1 inhibition as a promising strategy to alleviate Mo/Cd-induced hepatotoxicity by restoring mitochondrial homeostasis.

To Cite This Article: Bai H, Liu L, Xing C, Gao F, Jiang Z, Wang Y, Xiong Z, Dai X, Yang F and Cao H, 2026. Voltage-dependent anion channel 1(VDAC1)-mediated mitophagy: A potential therapeutic target for mitochondrial damage induced by molybdenum and cadmium co-exposure in sheep hepatocytes. Pak Vet J, 46(4): 961-971. http://dx.doi.org/10.29261/pakvetj/2026.090

INTRODUCTION

Molybdenum (Mo) is an essential trace element that is integrated into molybdenum enzyme to support the redox metabolic process; however, when the intake exceeds physiological needs, Mo may become toxic and pose a threat to the health of animals and humans (Huang *et al*., 2022). Cadmium (Cd) is widely used in industrial production because of its good corrosion resistance. It has a long half-life in living organisms and low removal efficiency. Therefore, it is easy to accumulate in living organisms, including accumulation in the body through the process of nutrient transfer in the food chain (Park *et al*., 2021; Gong *et al*., 2022). Against this background, the environmental coexistence of Mo and Cd is not just a theoretical hypothesis, but represents a realistic mixed exposure, which requires a systematic evaluation of their combined toxicity. Previous studies have shown that long-term exposure to these metals can lead to systemic and multi-organ damage—the most significant are liver damage, kidney damage and reproductive dysfunction, and clinical associations between hepatitis and fertility-related diseases have also been reported (Liu *et al*., 2019; Xu *et al*., 2021; Li *et al*., 2022). The situation of ruminants is more

complicated: because these changes are driven by microorganisms in the rumen, they tend to be more sensitive to heavy metals, and under wild conditions, contaminated feed materials and water sources are more likely to be ingested into the body. It follows that interrogating Mo-Cd synergism is a closer approximation to the exposure reality faced by ruminant species. The liver, repeatedly identified as a primary target tissue for both Mo and Cd, is therefore taken here as the focal organ, and hepatotoxic responses associated with Mo and Cd exposure in ruminants are examined accordingly.

As the body's primary detoxifying organ, the liver operates at a high metabolic pace and, by extension, demands substantial energy input to sustain biotransformation and other biosynthetic tasks. That energy is largely furnished by mitochondria—often described as cellular power units which, in hepatocytes, are also positioned as central governors of redox homeostasis, lipid handling, and regulated cell death. Under a broad spectrum of pressures nutrient deprivation, cellular aging and differentiation, disease-related insults, and exposure to exogenous chemicals—mitophagy is commonly engaged so that defective or surplus mitochondria can be removed and intracellular equilibrium preserved. Once mitochondrial quality deteriorates, hallmarks of dysfunction are typically observed, including electron leakage from the electron-transport chain, reactive oxygen species (ROS) generation, and, when damage escalates, progression toward cell death (Isaev *et al*., 2023). The outcome, however, is not always consistent. In certain contexts, activation of mitophagy occurs alongside compensatory mitochondrial biogenesis, which can, in effect, help preserve a relatively stable mitochondrial pool even as clearance continues (Palikaras *et al*., 2015). Too much of the same process, though, carries its own cost. When mitophagy is driven beyond adaptive needs, mitochondrial abundance may be reduced and residual organelles may function poorly, with the mitochondrial network losing coherence and hepatocellular fitness being eroded. Heavy metals have repeatedly been reported to perturb mitochondrial membrane permeability, amplify ROS formation, and provoke mitophagy beyond physiological range, a sequence that has been linked to disordered hepatic metabolism and hepatotoxic outcomes (Bai *et al*., 2021; Cui *et al*., 2021; Zhong *et al*., 2021; Zhang *et al*., 2024; Xiong *et al*., 2025). Even so, whether Mo and Cd can injure the ruminant liver through mitophagy induction—and, if so, through which defined molecular route remains to be clarified.

Mitophagy proceeds through at least two broad classes of routes: the canonical PTEN-induced kinase 1 (PINK1)/Parkin axis, and a set of ubiquitin-independent programs. Evidence from multiple studies has suggested that heavy-metal challenge is capable of engaging mitophagy not only through PINK1/Parkin signaling, but also through non-ubiquitin pathways mediated by receptors such as FUN14 domain-containing 1 (FUNDC1) and BCL2/adenovirus E1B 19 kDa-interacting protein 3 (BNIP3) (Kato *et al*., 2021; Bai *et al*., 2023; Lin *et al*., 2023). In this case, the mitochondrial outer membrane protein is by no means a passive bystander. They usually act as signaling elements and connecting components, sometimes even as receptor-like nodes, and can also participate in the renewal and degradation of proteins. Overall, these coordinated functions help to organize the mitophagy mechanism, thus maintaining the quality control of mitochondria and ultimately affecting the performance of organelles at the cellular level. In the outer membrane component, voltage-dependent anion channel 1 (VDAC1) exists as the main channel on the mitochondrial surface. It is often described as the "gatekeeper" of mitochondrial exchange, which regulates the flow of metabolites including pyruvate and ATP, and thus affects the biological energy output of cells (Shoshan-Barmatz *et al*., 2018; Verma *et al*., 2023). Another important significance is that VDAC1 is an important substrate of Parkin protein; in the process of regulating the balance between mitophagy and cell apoptosis, the ubiquitinization of VDAC1 has been considered a key regulatory step (Ham *et al*., 2020). Based on this view, heavy metal-related hepatotoxicity has been reported to be related to the upregulation of MUC and the stronger interaction between MUC and VDAC1, which is believed to push mitophagy beyond the adaptive limit (Liu *et al*., 2023). Notably, work by Sven Geisler and c colleagues also supports VDAC1 as an important target within PINK1/Parkin-mediated mitophagy (Geisler *et al*., 2010). Even with these observations in hand, the precise molecular steps by which VDAC1 contributes to hepatocyte mitophagy under combined Mo and Cd exposure remain insufficiently resolved.

Our earlier work has indicated that combined exposure to Mo and Cd is accompanied by a disruption of redox homeostasis, structural injury to mitochondria, and overt mitochondrial dysfunction (Wu *et al*., 2022; Xiong *et al*., 2025). However, the specific molecular mechanisms of VDAC1 involved in liver injury induced by co-exposure of Mo and Cd deserve further exploration. On this basis, we propose that VDAC1 operates as a central node in mitochondrial quality control; accordingly, suppression of VDAC1 would be expected to mitigate Mo/Cd-associated hepatotoxicity, at least in part, by re-establishing mitochondrial function and preserving mitochondrial dynamics. To test this, we modeled the hepatotoxicity of Mo and Cd co-exposure and evaluated the effects of the mitophagy inhibitor CsA and the VDAC1 inhibitor VBIT-4 on mitochondrial dynamics, biogenesis, and mitophagy. Our study found that inhibition of VDAC1 maintained the normal function and function of mitochondria under Mo and Cd co-exposure, and then alleviated liver toxicity.

MATERIALS AND METHODS

Cell isolation, culture, and treatment: The animal experiments and procedures were approved by the Ethics Committee of Jiangxi Agricultural University (Permission number: JXAULL-2020-04). We confirm that all one-day-old lambs were humanely euthanized under deep anesthesia to ensure a completely painless procedure. The process involved first inducing deep anesthesia with Xylazine (0.1-0.2mg/kg IM), followed by intravenous heparin sodium (1400IU/kg) administration to prevent coagulation for subsequent liver perfusion. Sheep hepatocytes were isolated by the improved collagenase perfusion method. In brief, the liver caudate lobe was removed from one day-old sheep in the sterile fume hood, rinsed of surface blood stains with preheated perfusion I (140mM NaCl, 6.7 mM KCl, 10mM HEPES, 5.5mM glucose, and 0.64mM EDTA). Next, the vessels with thick sections were selected to be irrigated with perfusion A at the flow rate of 50mL/min for 10-15 min until the liver turned earth yellow. Then, perfusion II (140mM NaCl, 6.7mM KCl, 30 mM HEPES, 5.5mM glucose, and 5mM $CaCl_2$) was applied at the flow rate of 50 mL/min for 5 min until the outflow liquid was clear. Finally, perfusion

III (0.1g IV collagenase was added into 0.5L perfusion II) was applied at the rate of 20mL/min, digestion was stopped and the collected cells were collected once the liver tissue became soft.

Cell grouping and processing: Mo and Cd stock solutions were prepared by dissolving 0.21g of $(NH_4)6Mo7O24{\cdot}4H_2O$ in 10mL of ultrapure water (120mmol L^{-1}), and 0.37g of $CdCl_2$ in 50mL of ultrapure water (40mmol L^{-1}), respectively. Cells were spread in plates (96-well plates), and after 80% cell polymerization, the cells were treated with Mo (0, 300, 600, 900, 1200, 1500, 1800μM) and Cd (0, 0.5, 1, 2, 4, 8, 16μM), and the half inhibition (IC_{50}) of sheep hepatocytes at 24 h of treatment with Mo and Cd was measured by CCK-8 method. The specific procedure was described in the instruction manual (Abkine Scientific Co., Ltd, China).

According to IC_{50}, sheep hepatocytes were exposed to 600μM Mo, 4μM Cd, 1μM CsA, and 100μM VBIT, treated individually or in combination as needed.

Transmission electron microscope (TEM) observation: Referring to the previous method, cells were collected and immobilized with 2.5% glutaraldehyde for 24h and 2% osmium acid. for 2h (Liu *et al*., 2022). After embedding the sections and staining, image acquisition was performed using the TEM (HT7700; Hitachi, Japan).

Immunofluorescence detection: Briefly, mitochondria and lysosomes of sheep hepatocytes were labeled with MitoTracker Green (80nm, 15min) and LysoTracker Red (50nm, 15min) fluorescent probes, respectively. Images were collected using a NIKON Eclipse confocal laser scanning microscope. MitoTracker Green was excited at 488nm, and signals were recorded in the 500–550nm band; LysoTracker Red was excited at 561nm, with emission captured at 570–620nm. Representative fields were imaged, and colocalization was quantified in ImageJ by calculating Pearson's correlation coefficient (Yang *et al*., 2021).

Assessment of mitochondrial respiratory function: Cellular mitochondria were isolated strictly according to the manufacturer's instructions (Beyotime, China). Oxygen consumption was subsequently measured with a Clark-type oxygen electrode (Hansatech, UK), using procedures aligned with those reported previously (Lu *et al*., 2018).

Flow cytometry: Following the indicated treatments, cells were incubated with the JC-1 fluorescent probe at 37°C for 15 min in accordance with the manufacturer's protocol. Cells were then harvested by centrifugation, and pellets were washed twice with JC-1 staining buffer. Mitochondrial membrane potential (MMP) was then evaluated by flow cytometry.

In addition, following treatment, cells were washed twice with PBS and harvested by centrifugation for downstream analyses. The pellet was then incubated with 2',7'-dichlorodihydrofluorescein diacetate (DCFH-DA) probe diluted in culture medium, was swollen, with vacuolation and cristae rupture. Following incubation, reactive oxygen species (ROS) levels were quantified via flow cytometry.

ATP content analysis: Following the preparation of reagents as specified in the ATP assay kit (Nanjing Jiancheng, China), hepatocytes were homogenized in boiled double-distilled water. The resulting homogenate was heated in a boiling water bath for 10 minutes, followed by centrifugation to collect the supernatant. ATP levels were then quantified using an enzyme-labeled instrument according to the kit protocol.

The determination of mtDNA copy number: Mitochondrial DNA (mtDNA) was extracted according to the instructions (Beyotime, China). Mitochondrial coding gene D-loop was selected to represent mitochondrial gene (mtDNA) and β-actin was selected to represent the nuclear gene (nDNA). mtDNA copy number was represented by the ratio of mitochondrial gene to nuclear gene fluorescence quantification. The primer sequences of all mRNA are shown in Table 1.

RT-qPCR analysis: Based on the reference (Miao *et al*., 2022), total RNA was isolated from hepatocytes using Trizol reagent (Takara, Japan), and cDNA was synthesized using the PrimeScript® RT Reagent Kit following the manufacturer's protocol. The resulting cDNA was amplified with gene-specific primer pairs (Table 1) that were designed against ovine sequences downloaded from NCBI (GenBank IDs listed) with the aid of NCBI Primer-BLAST and synthesized by Wuhan Tsingke Biological Technology Co., Ltd. RT-qPCR was performed on an ABI 7900HT system (Applied Biosystems, USA) using SYBR Green Master Mix in a two-step protocol: 95°C for 30s, followed by 40 cycles of 95°C for 5s and 60°C for 32s (annealing temperature validated for all primers). Relative mRNA abundance was calculated by the $2^{-\Delta\Delta CT}$ method with GAPDH as the reference gene.

Table 1: qRT-PCR Primer sequences

Genes	Forward primer	Reverse primer	GenBank ID
D-Loop	AGCCAGTTGAACACCCCTAC	GACCCAGGTGCCTATATATTTACTTC	AF 010406.1
β-actin	CAGTCGGTTGGATCGAGCAT	AGAAGGAGGGTGGCTTTTGG	NM_001009784.3
LC3A	GTCACCCAGGCGAGTTACC	GCTTCTCACCCTTGTAGCGT	XM_015099492.3
LC3B	AGCTCCAAGTGAGCACATTCA	AGGAGCGTCCTCCAATTGAC	XM_004014953.4
PINK1	CTGATGGCTCCTGAGAGGC	TTCTCCGTCAGTCTGTTGGC	XM_042244672.1
Parkin	CTGGGACCAGAGCGGAATTT	GTCACGCAGTACAGGTGGAA	XM_027972640.2
P62	GATCCCCGGCTGATTGAGTC	TGTGTGAGCAGACATCGTCA	XM_042249330.1
VDAC1	CGACGCTTCCGAGCAGA	AGCCTTCATAACCCAGCACC	XM_015095469.3
Drp1	GCTGGAGAAGAGGAATCGCAT	GCAGCCATTTCAAAACCCAGG	XM_015094867.3
Fis1	AGGCCATGAAGAAAGATGGACT	GACGTTCACAGAGGACAGGG	XM_027961118.2
Mfn1	CTTTTGAGGAGTGTATCTCGCAG	GTCCAGTATGTTTTTCACAGTGTCT	XM_004003134.5
Mfn2	CACCATCGGAAAACGCGA	TGGGTCCAGTTCTGCATTCC	XM_004013713.5
OPA1	TAAGGATTGGCAGACCTCGC	CTTCCACTCCTCGAGACTCC	XM_027957232.2
PGC-1α	TGACATCGAGTGTGCTGCT	TGAGGGCAATCCGTCTTCAT	XM_004009738.5
GAPDH	AGAGTGAGTGTCGCTGTTGAAGT	TCCGTTGTGGATCTGACCTG	XM_027961471.2

Western blot analysis: Based on the reference(Bai *et al*., 2021), PVDF membranes were incubated with different primary antibodies: LC3B (1:2000, ab192890, rabbit, Abcam, UK), Pink1 (1:1000, WL04963, rabbit, Wanleibio, China), Parkin (1:1000, WL02512, rabbit, Wanleibio, China), p62 (1:5000, H00008878-M01, Mouse, Novus Biologicals, USA), VDAC1 (1:1000, WL02790, rabbit, Wanleibio, China), Drp1 (1:500, WL03028, rabbit, Wanleibio, China), Fis1 (1:2000, ab156865, rabbit, Abcam, UK), Mfn2 (1:2000, 12186-1-AP, rabbit, Proteintech, USA),PGC-1α (1:1000, 66369-1-Ig, rabbit, Proteintech, USA), and GAPDH (1:1 000, 60004-1-Ig, mouse, Proteintech, USA). All primary antibodies were used under dilutions and catalog numbers indicated and had been validated for Western blot by the respective suppliers. After washing, membranes were incubated with secondary antibody for 1 hour, treated with ECL, and visualized using the BioRad Chemi Doc XRS system. Band intensity was quantified using ImageJ software.

Statistical analysis: Data were collected from at least three independent replicates and expressed as mean±Standard deviation (SD). Statistical significance was assessed using a two-tailed unpaired Student's t test or one-way analysis of variance (ANOVA), as appropriate for the dataset. If ANOVA revealed an overall group effect, Tukey's or Dunnett's post hoc multiple-comparison procedures were used. Differences were considered statistically significant at $P<0.05$. All statistical analyses and figure generation were performed in SPSS (version 22.0) and GraphPad Prism (version 8.0).

RESULTS

Sheep hepatocyte isolation and optimization of Mo/Cd exposure: To confirm that the isolated cells were sheep hepatocytes, primary cultures were established, and morphology was recorded at 0, 12, 24 and, 48 h after seeding (Fig. 1B). At the time of plating (0h), most cells appeared as single, translucent, spherical units with relatively uniform size and morphology. By 12h, nuclei became readily discernible and the cytoplasm appeared abundant; binucleated or multinucleated cells could be observed, and cell–cell contacts began to develop, giving rise to islet-like aggregates. At 24h, adhesion was largely completed (approximately 90% of cells), with cells adopting a flattened, thin morphology and forming lamellar junctions. After 48h of culture, cells had further spread and displayed firm attachment to the culture surface. Because hepatocytes are capable of glycogen storage, Periodic acid–Schiff (PAS) staining was performed; the appearance of distinctly bright purplish-red glycogen granules within the cytoplasm was taken as a positive reaction (Fig. 1C). In parallel, immunofluorescence analysis demonstrated CK18 (cytokeratin-18) positivity after 24h of culture, supporting successful hepatocyte isolation and providing the basis for subsequent experiments (Fig. 1D).

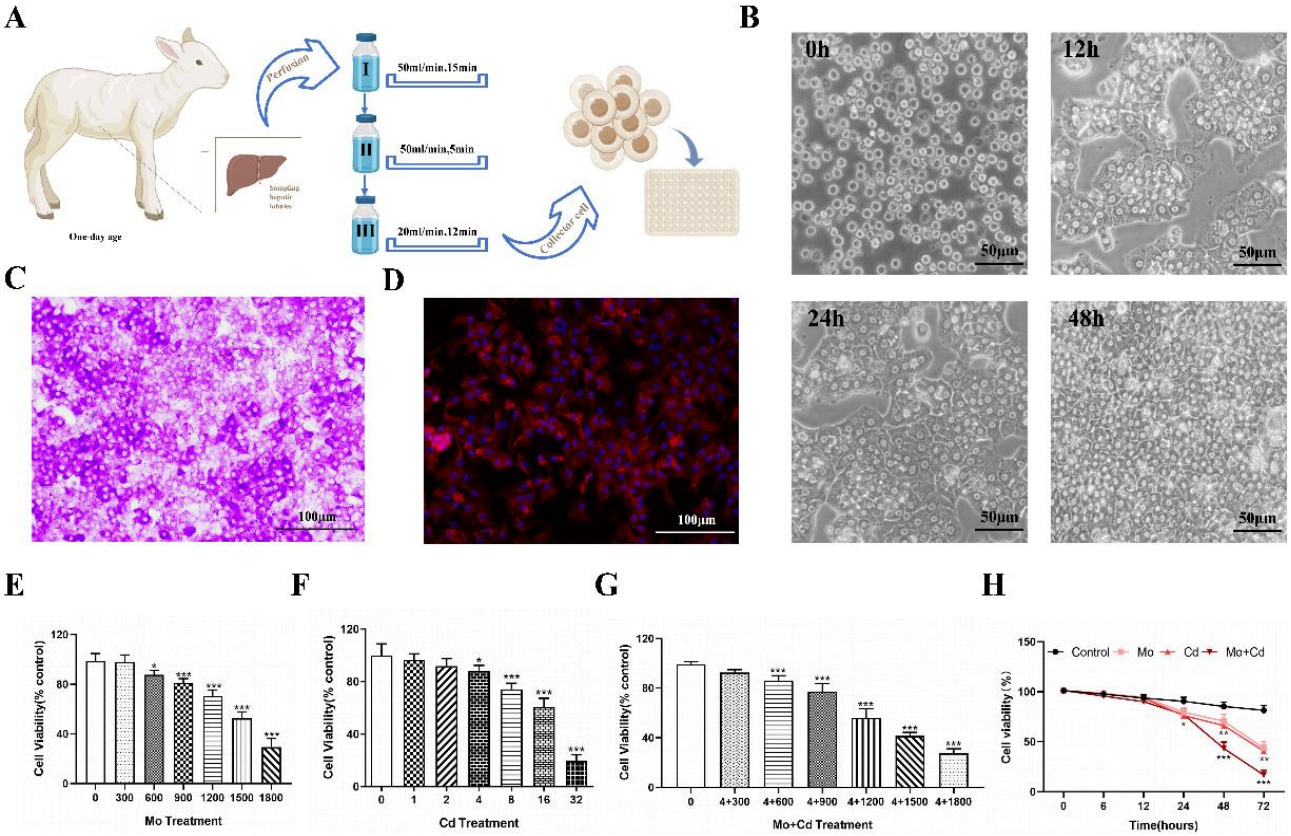

Fig.1: Isolation, culture, and identification of sheep preliminary hepatocytes, determination of molybdenum (Mo) and cadmium (Cd) attack concentration. (A) Cell extraction flow chart. (B) The growth of sheep hepatocytes at different times (200×). (C) Periodic acid–Schiff (PAS) staining of sheep hepatocytes. (D) Cytokeratin 18 (CK18) immunostaining of sheep hepatocytes. (E) Cell survival rate after Mo treatment. (F) Cell survival rate after Cd treatment. (G) Cell survival rate after combined treatment with Mo and Cd. (H) Cell survival rate after different treatments. Data were represented as mean ± SD of at least three independent experiments. "*" indicates significant difference compared with control group ($^{*}P<0.05$, $^{**}P<0.01$ and $^{***}P<0.001$). "#" indicates significant difference between corresponding group ($^{\#}P<0.05$, $^{\#\#}P<0.01$ and $^{\#\#\#}P<0.001$).

The half-maximal inhibitory concentrations (IC_{50}) of Mo and Cd in sheep hepatocytes were determined to be 1114μmol/L and 22.41μmol/L, respectively. In the Mo-treated cells, viability began to decrease significantly at 600μmol/L (Fig. 1E), whereas a pronounced reduction was first observed at 4μmol/L in the Cd-treated cells (Fig. 1F). As Mo or Cd concentrations increased stepwise, cell survival decreased in parallel, indicating a clear dose-dependent trend. Based on these findings, 600μmol/L Mo and 4μmol/L Cd were chosen for subsequent experiments (Fig. 1G). Of note, co-exposure to Mo and Cd led to a further reduction in cell viability at 24h (Fig. 1H).

Mo- and/or Cd-induced mitochondrial injury in sheep hepatocytes: To determine whether Mo and/or Cd exposure compromises mitochondrial integrity in hepatocytes, we performed ultrastructural analyses. In control cells, nuclear architecture remained intact, and mitochondria appeared densely packed and orderly in cross-section (Fig. 2A). Following Mo and/or Cd treatment, mitochondria showed clear pathological changes, including swelling, vacuolization, and disrupted or fragmented cristae. Moreover, mitophagosomes were detected in the Mo+Cd group.

To see whether these structural alterations translated into functional deficits, we next assessed a panel of mitochondrial indices. Relative to the control group, mitochondrial membrane potential (MMP) was significantly reduced (Figs. 2B–C), as were ATP content (Fig. 2E) and respiratory control ratio (RCR) as well as oxidative phosphorylation rate (OPR) (Figs. 2F–G). By contrast, intracellular ROS levels rose markedly (Fig. 2D), and mtDNA copy number was also increased (Fig. 2H). Overall, these results indicate that exposure to Mo and/or Cd triggers mitochondrial injury in sheep hepatocytes and is accompanied by quantifiable mitochondrial dysfunction.

Mo and/or Cd perturbed mitochondrial dynamics, suppressed biogenesis, and activated mitophagy in sheep hepatocytes: Mitochondrial turnover was first evaluated by confocal microscopy after staining cells with MitoTracker Green and LysoTracker Red. Compared with the control group, Mo- and/or Cd-treated cells showed a higher abundance of mitophagosomes (Figs. 3A–B). This was accompanied by an increased Pearson's correlation coefficient, indicating stronger mitochondria–lysosome colocalization (Fig. 3B).

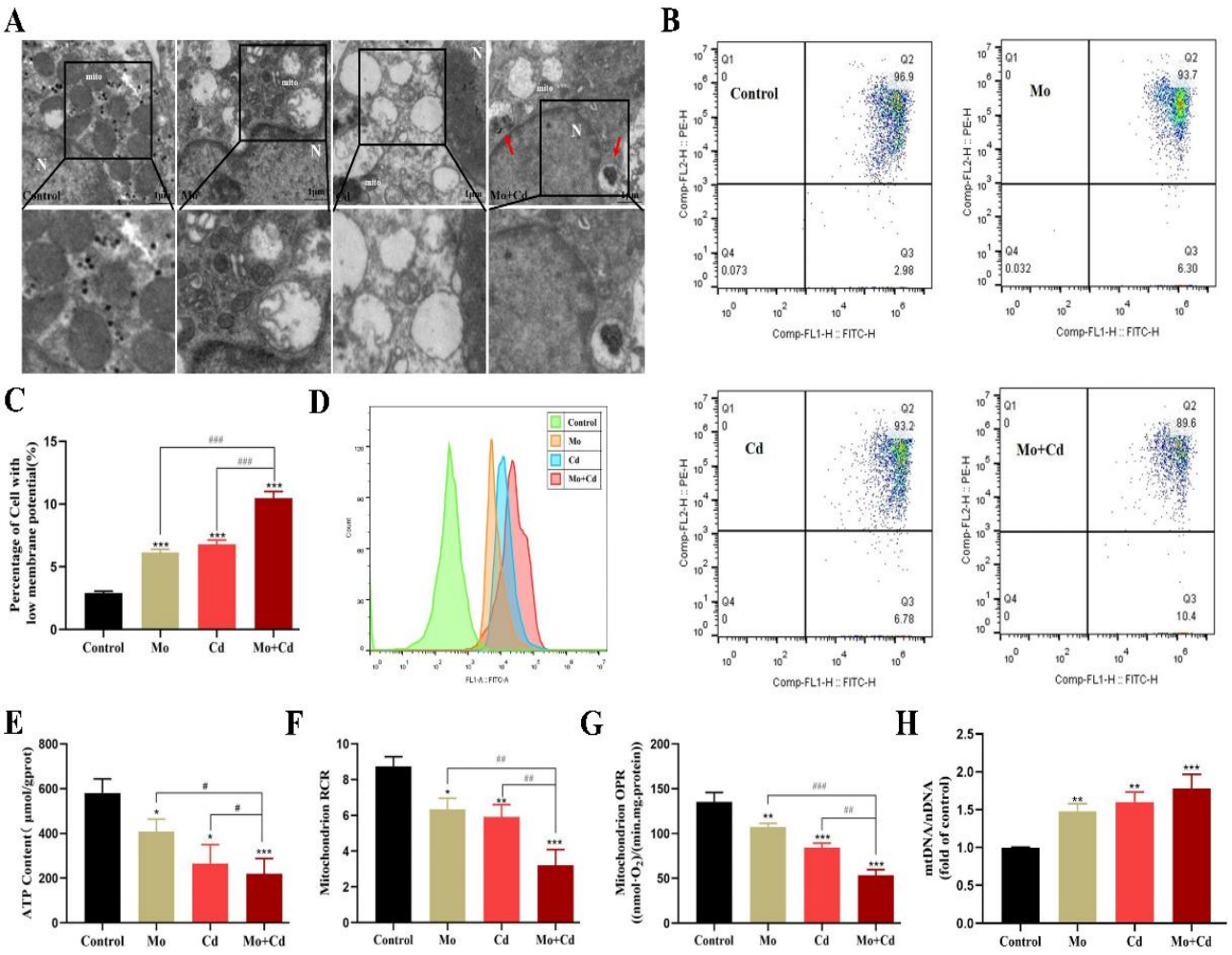

Fig.2: Mo or/and Cd-induced mitochondrial damage in sheep hepatocytes. (A) Ultrastructure of the sheep hepatocyte. Red arrows indicate mitophagosomes. "N" means nucleus, "mito" means mitochondrion. TEM ×10 000. The scale bar is 1μm. (B, C) Mitochondrial membrane potential (MMP) level. (D) Reactive oxygen species (ROS) production level. (E) Adenosine triphosphate (ATP) content. (F) Mitochondrial respiratory control ratio (RCR). (G) Mitochondrial oxygen consumption rate (OPR0. (H) The number of mitochondrial DNA (mtDNA) copy. Data were represented as mean ± SD of at least three independent experiments. "*" indicates significant difference compared with control group ($^{*}P<0.05$, $^{**}P<0.01$ and $^{***}P<0.001$). "#" indicates significant difference between corresponding group ($^{*}P<0.05$, $^{**}P<0.01$ and $^{***}P<0.001$).

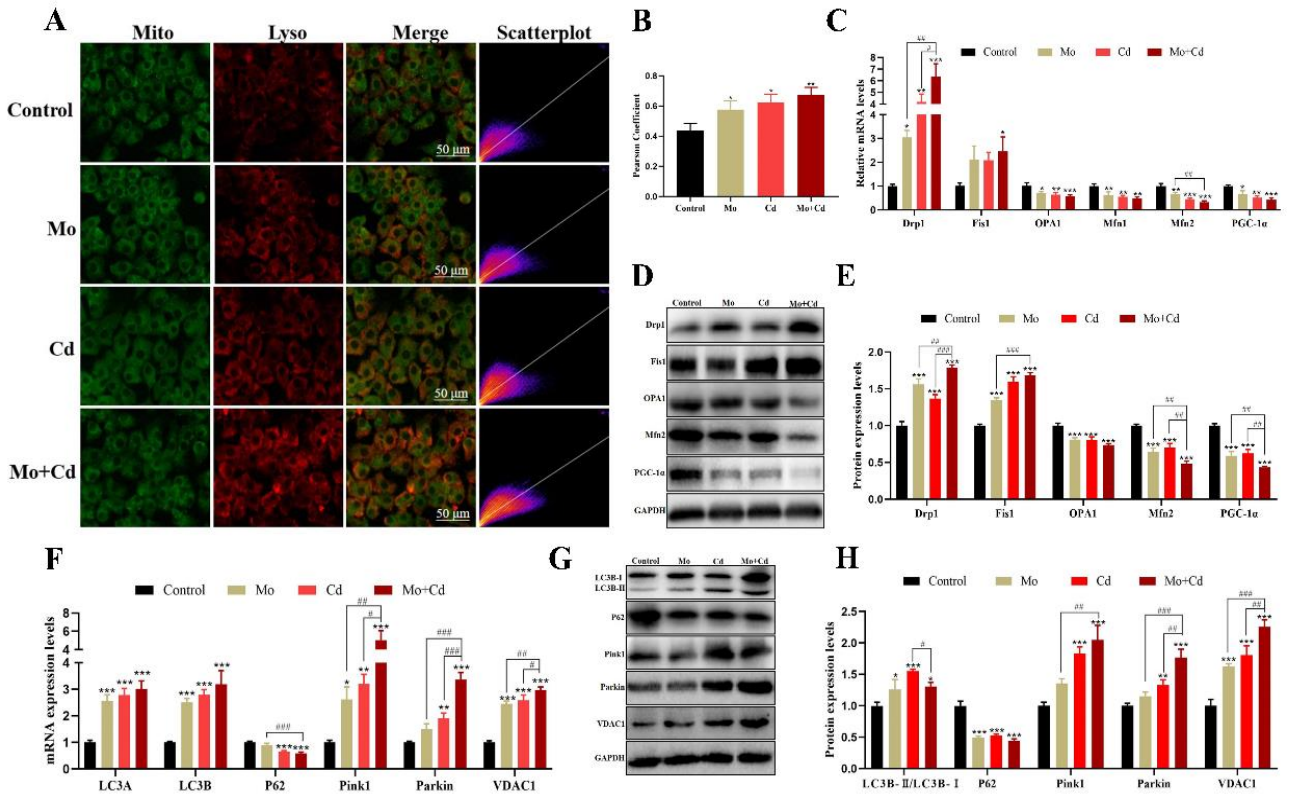

Fig.3: Mo or/and Cd disrupted mitochondrial dynamics, reduced mitochondrial biogenesis, and induced mitochondrial autophagy in sheep hepatocytes. (A) Colocalization of mitochondria and lysosomes by immunofluorescence. (B) Pearson correlation coefficient. (C) The mRNA levels of mitochondrial division, fusion, and biogenesis-related genes. (D, E) Expression levels of mitochondrial division, fusion, and biogenesis-related proteins. (F) The mRNA levels of mitophagy-related genes. (G, H) Expression levels of mitophagy-related proteins. Data were represented as mean ± SD of at least three independent experiments. "*" indicates significant difference compared with control group ($^{*}P<0.05$, $^{**}P<0.01$ and $^{***}P<0.001$). "#" indicates significant difference between corresponding group ($^{\#}P<0.05$, $^{\#\#}P<0.01$ and $^{\#\#\#}P<0.001$).

Changes in mitochondrial dynamics were then assessed. In the Mo+Cd group, both mRNA and protein levels of the fission-associated markers Drp1 and Fis1 were increased, whereas the fusion-related factors OPA1, Mfn1, and Mfn2 were reduced. In parallel, expression of the mitochondrial biogenesis regulator PGC-1α was significantly decreased at both the transcript and protein levels (Figs. 3C–E). Mitophagy-associated readouts were further evaluated, showing elevated mRNA expression of LC3A, LC3B, Pink1, Parkin, and VDAC1 in the Mo+Cd group, while P62 mRNA was reduced (Fig. 3F). Consistently, LC3B-II/LC3B-I ratio as well as protein levels of Pink1, Parkin, and VDAC1 were increased, with a concomitant decrease in P62 protein abundance (Figs. 3G–H). Collectively, these results support that exposure to Mo and/or Cd disrupts mitochondrial fission–fusion balance, attenuates mitochondrial biogenesis, and promotes mitophagy in sheep hepatocytes.

CsA aggravates Mo/Cd co-exposure–associated mitochondrial dysfunction in hepatocytes: To probe whether mitophagy contributes to the mitochondrial phenotype observed under combined Mo and Cd exposure, cyclosporin A (CsA) was administered as an inhibitor of mitophagy. In hepatocytes challenged with Mo and Cd, CsA treatment was accompanied by a pronounced reduction in mitophagosome formation; meanwhile, mitochondrial ultrastructural injury appeared more severe, as reflected by enhanced vacuolization and increased fragmentation (Fig. 4A).

Mirroring the morphological shifts described previously, the Mo+Cd+CsA group demonstrated a more pronounced depletion of MMP (Figs. 4B–C) coupled with a surge in ROS accumulation compared to the Mo+Cd group (Fig. 4D). This physiological strain was reflected in the bioenergetic profiles as well; specifically, ATP content, the RCR, and the OPR all underwent significant reductions (Figs. 4E–G), while mtDNA copy number paradoxically rose (Fig. 4H). From this perspective, it appears that while CsA is effective in blocking mitophagosome formation, its presence ultimately intensifies the deterioration of mitochondrial function in hepatocytes subjected to simultaneous Mo and Cd exposure.

CsA suppresses Mo/Cd-triggered mitophagy and perturbs mitochondrial homeostasis: In cells receiving CsA in the setting of Mo and Cd co-exposure, fewer mitochondria–lysosome fluorescent aggregates were observed (Fig. 5A). Consistent with this qualitative change, Pearson's correlation coefficient showed a downward trend relative to the Mo+Cd group, although the difference did not reach statistical significance (Fig. 5B).

Mitochondrial dynamics were subsequently examined. Relative to Mo+Cd treatment alone, the Mo+Cd+CsA group showed higher Drp1 mRNA, while OPA1 and Mfn2 transcripts were reduced (Fig. 5C). At the protein level, shifts in Drp1 and Fis1 aligned with this transcriptional trend (Figs. 5D–E). Meanwhile, PGC-1α abundance declined even further, which, from this perspective, is consistent with an added constraint on mitochondrial biogenesis.

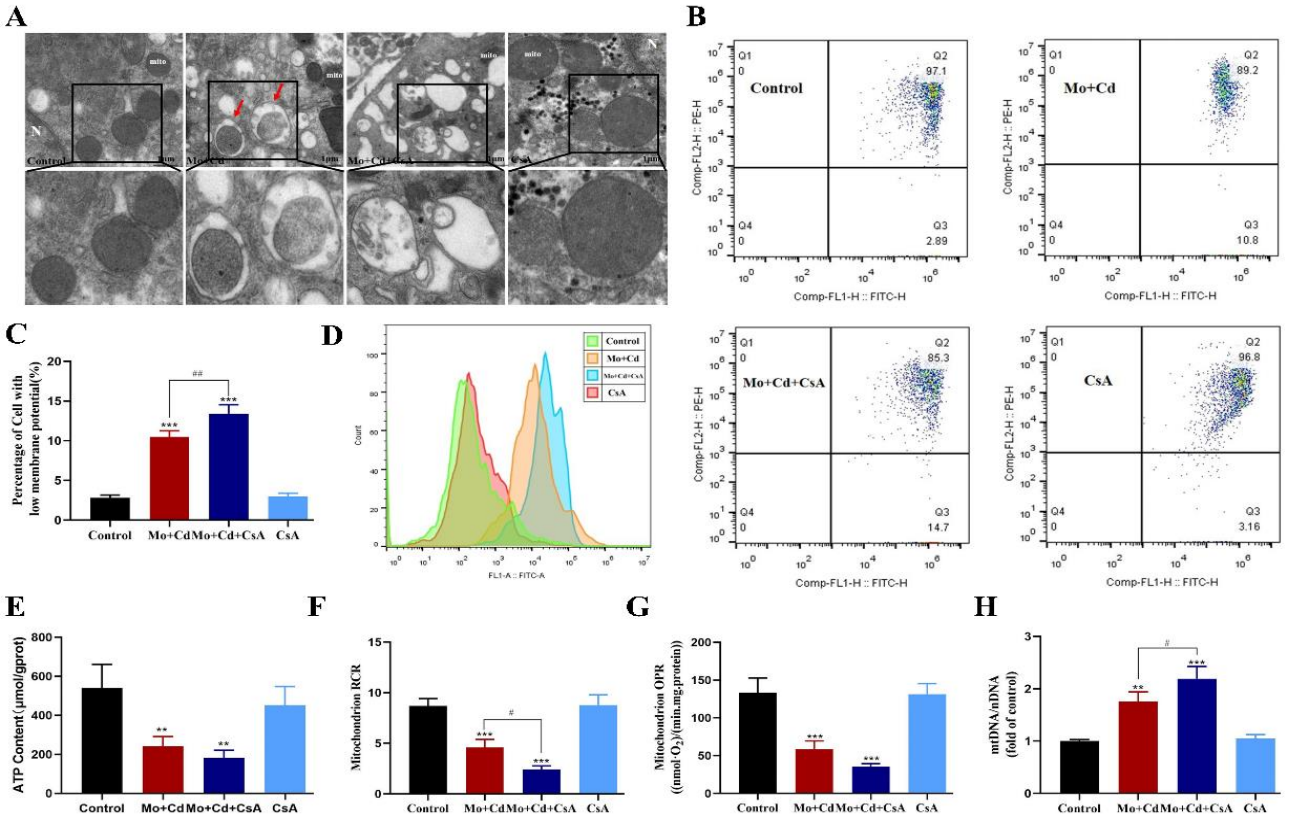

Fig.4: The addition of cyclosporin A (CsA) aggravated the mitochondrial function damage induced by Mo and Cd in sheep hepatocytes. (A) Ultrastructure of the sheep hepatocytes. Red arrows indicate mitophagosomes. "N" means nucleus, "mito" means mitochondrion. TEM ×10 000.The scale bar is 1μm. (B, C) MMP level. (D) ROS production level. (E) ATP content. (F) Mitochondrial RCR. (G) Mitochondrial OPR. (H) The number of mtDNA copies. Data were represented as mean ± SD of at least three independent experiments. "*" indicates significant difference compared with control group (*P<0.05, **P<0.01 and ***P<0.001). "#" indicates significant difference between corresponding group (*P<0.05, **P<0.01 and ***P<0.001).

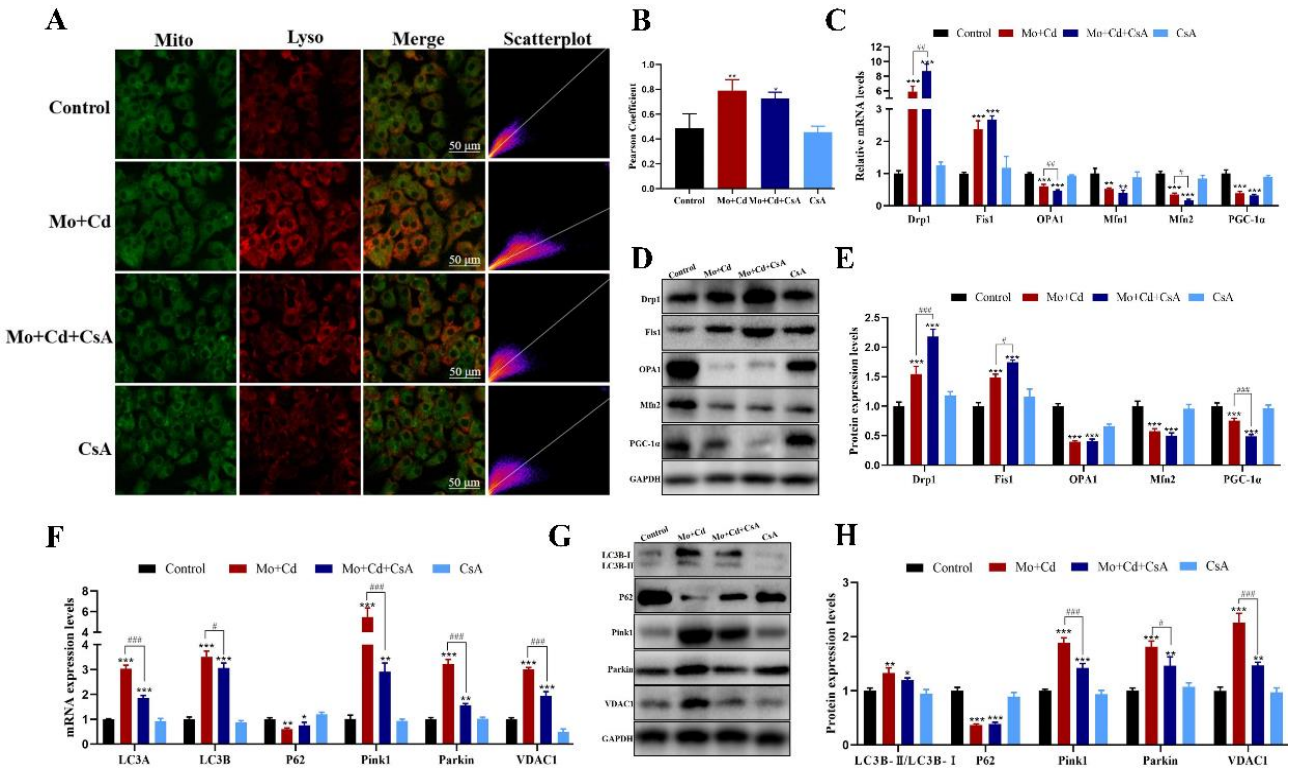

Fig.5: The addition of CsA alleviated mitophagy induced by Mo and Cd in sheep hepatocytes. (A) Colocalization of mitochondria and lysosomes by immunofluorescence. (B) Pearson correlation coefficient. (C)The mRNA levels of mitochondrial division, fusion, and biogenesis-related genes. (D, E) Expression levels of mitochondrial division, fusion, and biogenesis-related proteins. (F) The mRNA levels of mitophagy-related genes. (G, H) Expression levels of mitophagy-related proteins. Data were represented as mean ± SD of at least three independent experiments. "*" indicates significant difference compared with control group (*P<0.05, **P<0.01 and ***P<0.001). "#" indicates significant difference between corresponding group (*P<0.05, **P<0.01 and ***P<0.001).

Mitophagy-related gene expression—including LC3A, LC3B, Pink1, Parkin, and VDAC1—was markedly suppressed after CsA administration under Mo/Cd co-exposure (Fig. 5F). By comparison, P62 mRNA did not show a clear change. Immunoblotting results largely echoed these patterns, with a reduced LC3II/LC3I ratio and lower Pink1, Parkin, and VDAC1 protein levels; notably, P62 protein increased (Figs. 5G–H). Collectively, these results indicate that CsA dampens Mo/Cd-induced mitophagy but is associated with a worsening of mitochondrial fission–fusion imbalance and further impairment of mitochondrial biogenesis.

VDAC1 inhibition mitigates Mo/Cd-associated mitochondrial dysfunction in hepatocytes: To examine the mitochondrial consequences of targeting VDAC1 in ovine hepatocytes, the VDAC1 inhibitor VBIT-4 (denoted as "VBIT" in the figures) was administered. Under Mo+Cd co-exposure, VBIT-4 led to a marked reduction in mitophagosome abundance and was accompanied by an attenuation of mitochondrial vacuolization and fragmentation (Fig. 6A).

Functionally, MMP was significantly higher in the Mo+Cd+VBIT-4 (VBIT) group than in the Mo+Cd group (Figs. 6B–C). In parallel, ROS accumulation was substantially decreased following VBIT-4 treatment (Fig. 6D), whereas ATP content was increased (Fig. 6E). Although respiratory control ratio (RCR) and oxidative phosphorylation rate (OPR) showed upward trends after VBIT-4 administration, the differences relative to Mo+Cd treatment alone did not reach statistical significance (Figs. 6F–G). By contrast, mtDNA copy number was reduced in the Mo+Cd+VBIT-4 (VBIT) group compared with the Mo+Cd group (Fig. 6H).

VDAC1 inhibition blunts Mo/Cd-induced mitophagy and shifts mitochondrial dynamics toward fusion and biogenesis in sheep hepatocytes: In the Mo+Cd+VBIT-4 (VBIT) group, mitochondria–lysosome fluorescent aggregates were visibly reduced (Fig. 7A). Pearson's correlation coefficient also trended downward relative to the Mo+Cd group, although this change did not reach statistical significance (Fig. 7B). At the transcriptional level, Drp1 and Fis1 mRNA abundance was decreased compared with Mo+Cd exposure alone (Fig. 7C). Consistent with this pattern, Drp1 and Fis1 protein levels were reduced, whereas the fusion-associated proteins Mfn2 and Opa1, together with the biogenesis regulator PGC-1α, were significantly elevated in the Mo+Cd+VBIT-4 (VBIT) group (Figs. 7D–E).

Mitophagy-related readouts were similarly affected. Relative to the Mo+Cd group, mRNA levels of LC3B, Pink1, Parkin, and VDAC1 were markedly lower following VBIT-4 treatment (Fig. 7F). Immunoblotting further demonstrated decreases in LC3II/LC3I as well as in Pink1, Parkin, and VDAC1 protein abundance in the Mo+Cd+VBIT-4 (VBIT) group (Figs. 7G–H). Taken together, these findings indicate that inhibition of VDAC1 attenuates Mo/Cd-evoked mitophagy and is associated with reduced mitochondrial fission, enhanced fusion, and partial restoration of mitochondrial biogenesis in sheep hepatocytes.

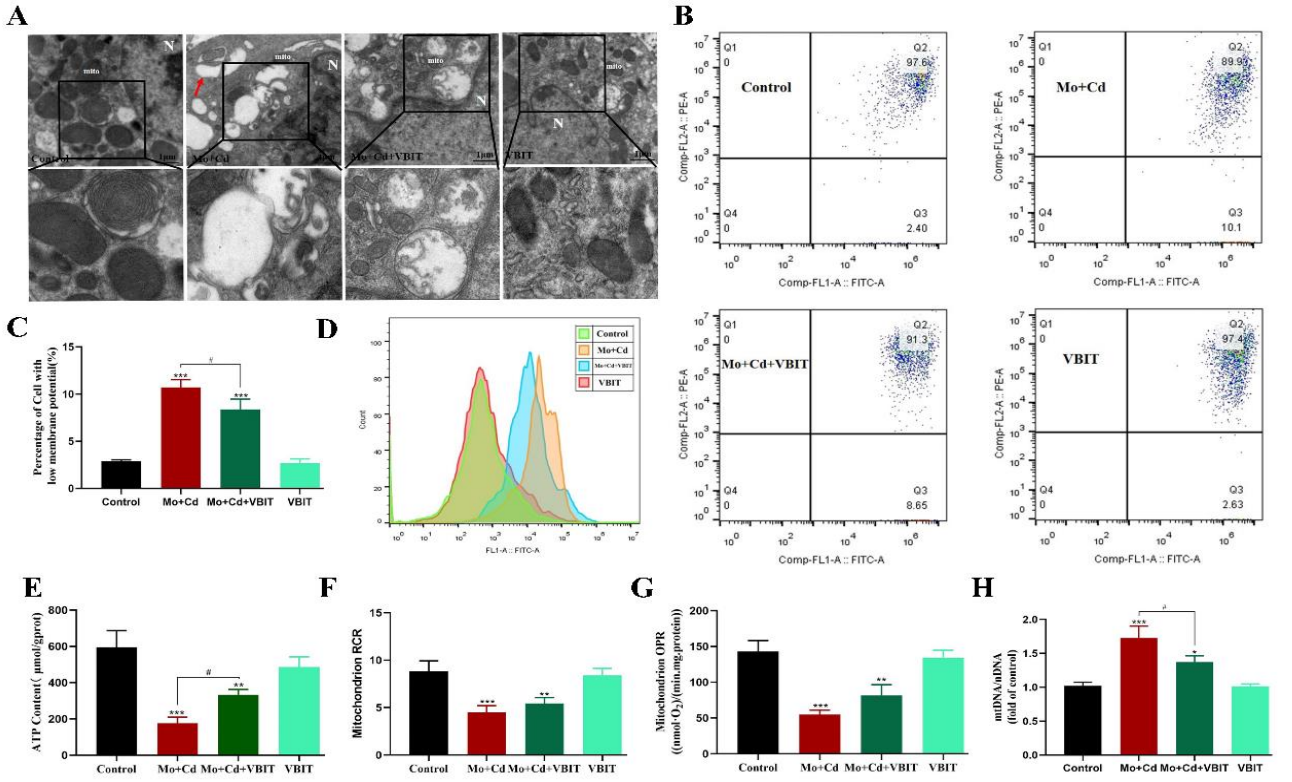

Fig.6: The addition of VBIT-4 alleviated the mitochondrial functional damage induced by Mo and Cd in sheep hepatocytes. (A) Ultrastructure of the sheep hepatocyte. Red arrows indicate mitophagosomes. "N" means nucleus, "mito" means mitochondrion. TEM ×10 000. The scale bar is 1 μm. (B, C) MMP level. (D) ROS production level. (E) ATP content. (F) Mitochondrial RCR. (G) Mitochondrial OPR. (H) The number of mtDNA copy. Data were represented as mean ± SD of at least three independent experiments. "*" indicates significant difference compared with control group ($^{*}P<0.05$, $^{**}P<0.01$ and $^{***}P<0.001$). "#" indicates significant difference between corresponding group ($^{*}P<0.05$, $^{**}P<0.01$ and $^{***}P<0.001$). In this figure, 'VBIT' refers to VBIT-4.

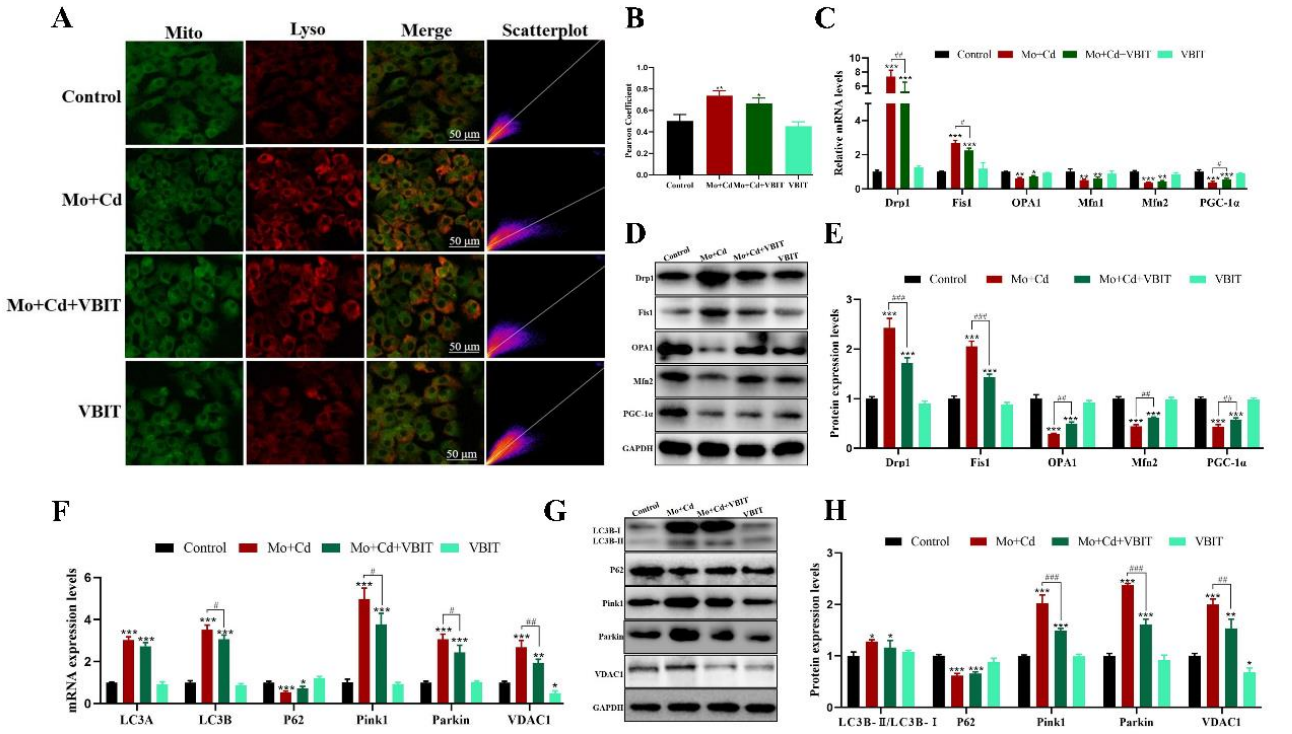

Fig.7: The addition of VBIT-4 alleviated the effects of Mo and Cd co-induced on mitophagy, kinetic disruption, and biogenesis in sheep hepatocytes. (A) Colocalization of mitochondria and lysosomes by immunofluorescence. (B) Pearson correlation coefficient. (C) The mRNA levels of mitochondrial division and fusion, and mitochondrial biogenesis-related genes. (D, E) Expression levels of mitochondrial division and fusion and mitochondrial biogenesis-related proteins. (F) The mRNA levels of mitophagy-related genes. (G, H) Expression levels of mitophagy-related proteins. Data were represented as mean ± SD of at least three independent experiments. "*" indicates significant difference compared with control group ($^{*}P<0.05$, $^{**}P<0.01$ and $^{***}P<0.001$). "#" indicates significant difference between corresponding group ($^{\#}P<0.05$, $^{\#\#}P<0.01$ and $^{\#\#\#}P<0.001$). In this figure, 'VBIT' refers to VBIT-4.

DISCUSSION

Since the pre-industrial era, the exponential increase in environmental pollution from Mo and Cd has been highlighted by Genchi et al, underscoring the growing environmental stressors (Geisler *et al*., 2010). Once released into the environment, these metals can be transferred through trophic pathways and accumulate in animals, thereby posing a potential threat to livestock production and the sustainability of the farming sector. Through the study using ruminants as a model, we observed that the exposure of Mo and Cd coincided with the obvious mitochondrial ultrastructure damage of sheep liver cells, while there were a disorder of division-fusion regulation and the appearance of seemingly excessive mitophagy. Interestingly, although CsA inhibits mitophagy, it does not restore mitochondrial function or rebalance mitochondrial dynamics, nor does it significantly enhance mitochondrial production. In contrast, VBIT supplements not only inhibit mitophagy, but also improve mitochondrial properties, and mitochondrial dynamic balance is basically maintained.

Exposure to heavy metals (including Mo and Cd) has long been associated with mitochondrial damage, which is usually manifested by increased mtROS, changes in MMP and decreased intracellular ATP levels (Wei *et al*., 2022). The observations in our research are consistent with this series of studies: when sheep liver cells are exposed to Mo and Cd at the same time, the redox balance is destroyed, which is manifested in the weakening of antioxidant ability and increased oxidative stress. It can be reasonably inferred that this oxidation burden leads to the loss of the integrity of the mitochondrial ultrastructure observed here. Consistent with this explanation, the RCR and OPR—two indicators widely used to evaluate mitochondrial respiration (Wei *et al*., 2022)—decreased after Mo/Cd treatment, which coincided with the impaired activity of the electron transfer chain. Once the integrity of mitochondria is damaged, mtDNA is easier to release, and mtDNA is a recognized trigger for the inflammatory signaling pathway. Such damage to mitochondrial integrity can facilitate the release of mtDNA, a known trigger of inflammatory pathways. Intriguingly, we observed a significant increase in mtDNA copy number under stress conditions. We propose this may represent a compensatory mechanism where the organism attempts to bolster the oxidative phosphorylation system in response to its weakening, a phenomenon that warrants further investigation in the context of heavy metal hepatotoxicity (Vellingiri *et al*., 2022). The significant increase in mtDNA copy number under Mo, Cd and their combined stress may be due to the fact that the antioxidant system is interfered with during stress, and the organism compensates for the weakened level of oxidative phosphorylation by increasing the level of the mtDNA replicative-transcriptional system. Based on the above, we concluded that co-exposure of Mo and Cd disrupted the balance of redox and the structural integrity of mitochondria in sheep hepatocytes, thereby inducing mitochondrial dysfunction.

Mitophagy serves as a cytoprotective mechanism that removes excess or dysfunctional mitochondria and maintains mitochondrial fine-tuning to balance intracellular homeostasis(Wang *et al*., 2023). However, its over-activation can lead to pathological outcomes. In line

with studies on heavy metal-induced hepatotoxicity (Chen *et al*., 2021; Liu *et al*., 2023; Li *et al*., 2024). We found that Mo and Cd activated the PINK1/Parkin-mediated mitophagy pathway in sheep hepatocytes, as indicated by increased levels of LC3A, LC3B, Pink1, and Parkin, and decreased P62. To clarify the contribution of excessive mitophagy, we applied the inhibitor CsA. The results showed that CsA effectively blunted the mitophagy induced by Mo and Cd. However, contrary to a purely protective role, CsA application unexpectedly aggravated mitochondrial dysfunction. This suggests that under the severe mitochondrial damage inflicted by Mo and Cd, the PINK1/Parkin-mediated mitophagy pathway may play a crucial, positive role in quality control by clearing damaged organelles. Inhibiting it with CsA might prevent the removal of excessively fragmented mitochondria, leading to the accumulation of toxic mitochondrial debris and amplifying the damage cascade, as similarly observed in other models of mitochondrial stress (Chen *et al*., 2021; Liu *et al*., 2023; Li *et al*., 2024). Hence, mitophagy plays a positive regulatory role in the mitochondrial quality control dysfunction in sheep hepatocytes caused by the co-exposure of Mo and Cd, and the inhibition of mitophagy may not be able to remove the accumulation of mitochondrial debris due to the excessive fragmentation, which further amplifies the downstream cascade of the mitochondrial damage response, and ultimately destroys the homeostasis of the mitochondrial quality control system and aggravates the mitochondrial dysfunction in sheep hepatocytes.

VDAC1 is involved in diverse cellular functions, including energy metabolism, mitochondria-mediated apoptosis, and mitophagy, making it a potential therapeutic target for various diseases (Ham *et al*., 2020; Hwang *et al*., 2021). More and more evidence shows that the overexpression of VDAC1 is associated with the pathological interaction of APP and Aβ. In this case, the conduction of mitochondrial channels may be hindered, resulting in reduced ATP production, increased oxidative stress, and reduced mitochondrial membrane integrity, these changes will eventually lead to mitochondrial dysfunction (Maimaiti *et al*., 2018; Lu *et al*., 2022). Against this background, it is reasonable to think that VDAC1 is not just a passive bystander, but plays an important role in hepatocyte disorders caused by Mo and Cd. Our data is consistent with this view, and more importantly, it also highlights a significant mechanical difference: although mitochondrial autophagy inhibitor cyclosporine A (CsA) and VDAC1 inhibitor VBIT-4 both reduce the indicators related to mitochondrial autophagy, their downstream functional results but it's completely different. CsA occurs with aggravated mitochondrial damage, while VBIT-4 produces a protective phenotype. This opposition shows that the initial damage in the Mo/Cd toxicity sequence is located upstream, that is, in or closely connected to VDAC1. We further proposed that VBIT-4 benefits by playing a role at this early node; by limiting the sub-polymerization of VDAC1, the mitochondrial membrane potential is maintained, ROS generation is inhibited, and mitochondrial dynamics change from excessive fission to fusion and generation (Shoshan-Barmatz *et al*., 2020). In addition, VBIT-4 normalized the Mo/Cd-associated increase in mtDNA copy number, which appears to reflect a compensatory response. Accordingly, rather than suppressing mitophagy in a broadly nonspecific way, as observed with CsA, VDAC1-directed inhibition is more consistent with intervention at an upstream control point—one that better preserves mitochondrial integrity and function by stabilizing fission–fusion balance and supporting biogenesis, thereby limiting progression toward maladaptive, excessive mitophagy.

Several limitations should be recognized. The present observations were obtained in an *in vitro* system using primary sheep hepatocytes; therefore, the extent to which these findings extrapolate to the intact liver, or to other species, remains to be established through additional validation. *In vivo*, responses to Mo/Cd exposure unfold within a far more complex physiological milieu—systemic inflammatory signaling, endocrine and metabolic regulation, and multicellular crosstalk between hepatocytes and non-parenchymal populations—which may substantially reshape the cellular effects described here.

In short, our research shows that mitochondrial autophagy plays a dual role in hepatotoxicity caused by Mo/Cd. More importantly, it reveals a key mechanism and treatment difference: extensive inhibition of mitochondrial autophagy with cyclosporine A is harmful, while inhibition of VDAC1 dimerization with VBIT-4 has a protective effect. This makes VDAC1 a promising therapeutic target, which can reduce the mitochondrial damage caused by heavy metals by accurately restoring the quality control balance without completely blocking the necessary mitochondrial autophagy removal pathway.

Conclusions*:* To synthesize, the study demonstrates that suppressing autophagy does not ameliorate the disturbances in mitochondrial dynamics and biogenesis that result from Mo and Cd co-exposure. Conversely, the suppression of VDAC1 significantly reduces mitophagy and the subsequent disturbances in mitochondrial dynamics and biogenesis triggered by Mo and Cd. These discoveries highlight VDAC1's promise as a target for therapeutic intervention and pave the way for further studies aimed at devising methods to neutralize the toxicity of Mo and Cd.

Acknowledgments: All authors thank all members of the team for their help in the experimental process in the clinical veterinary medicine laboratory at the College of Animal Science and Technology, Jiangxi Agricultural University.

Fundings*:* This work was supported by the National Natural Science Foundation of China (32460911), Natural Science Foundation of Jiangxi province (20242BAB26099), Position of Diseases Prevention and Control (JXARS-13) and the program of Modern Agricultural Industry Technology System of Cattle and Sheep and Jing gang Scholars Distinguished Professor Program of Jiangxi Provincial Colleges.

Data availability: Data will be made available on request.

Declaration of competing interests: The authors declare that they have no known competing financial interests or personal relationships that could have appeared to influence the work reported in this paper.

REFERENCES

Bai H, Fang Y, Cao H, *et al*., 2023. Inhibition of the BNIP3/NIX-dependent mitophagy aggravates copper-induced mitochondrial dysfunction in duck renal tubular epithelial cells. Environmental Toxicology 38:579-590.

Bai H, Yang F, Jiang W, *et al*., 2021. Molybdenum and cadmium co-induce mitophagy and mitochondrial dysfunction via ROS-mediated PINK1/Parkin pathway in Hepa1-6 cells. Ecotoxicology and Environmental Safety 224:112618.

Chen D, Ran D, Wang C, *et al*., 2021. Role of mitochondrial dysfunction and PINK1/Parkin-mediated mitophagy in Cd-induced hepatic lipid accumulation in chicken embryos. Life Sciences 284:119906.

Cui T, Jiang W, Yang F, *et al*., 2021. Molybdenum and cadmium co-induce hypothalamus toxicity in ducks via disturbing Nrf2-mediated defense response and triggering mitophagy. Ecotoxicology and Environmental Safety 228:113022.

Geisler S, Holmström KM, Skujat D, *et al*., 2010. PINK1/Parkin-mediated mitophagy is dependent on VDAC1 and p62/SQSTM1. Nature Cell Biology 12:119-131.

Gong Z, Zhao Y, Wang Z, *et al*., 2022. Epigenetic regulator BRD4 is involved in cadmium-induced acute kidney injury via contributing to lysosomal dysfunction, autophagy blockade and oxidative stress. Journal of Hazardous Materials 423:127110.

Ham SJ, Lee D, Yoo H, *et al*., 2020. Decision between mitophagy and apoptosis by Parkin via VDAC1 ubiquitination. Proceedings of the National Academy of Sciences of the United States of America 117:4281-4291.

Huang X, Hu D and Zhao F, 2022. Molybdenum: more than an essential element. Journal of Experimental Botany 73:1766-1774.

Hwang H, Shim JS, Kim D, *et al*., 2021. Antidepressant drug sertraline modulates AMPK-MTOR signaling-mediated autophagy via targeting mitochondrial VDAC1 protein. Autophagy 17:2783-2799.

Isaev NK, Stelmashook EV, Genrikhs EE, *et al*., 2023. Interaction between mitophagy, cadmium and zinc. Journal of Trace Elements in Medicine and Biology 79:127230.

Kato M, Abdollahi M, Tunduguru R, *et al*., 2021. miR-379 deletion ameliorates features of diabetic kidney disease by enhancing adaptive mitophagy via FIS1. Communications Biology 4:30.

Li J, Li M, Wang R, *et al*., 2024. Mitophagy protects against silver nanoparticle-induced hepatotoxicity by inhibiting mitochondrial ROS and the NLRP3 inflammasome. Ecotoxicology and Environmental Safety 273:116137.

Li Y, Liu H, He J, *et al*., 2022. The effects of oral administration of molybdenum fertilizers on immune function of Nanjiang brown goat grazing on natural pastures contaminated by mixed heavy metal. Biological Trace Element Research 200:2750-2757.

Lin S, Yang F, Hu M, *et al*., 2023. Selenium alleviates cadmium-induced mitophagy through FUNDC1-mediated mitochondrial quality control pathway in the lungs of sheep. Environmental Pollution 319:120954.

Liu C, Li H, Duan W, *et al*., 2023. MCU upregulation overactivates mitophagy by promoting VDAC1 dimerization and ubiquitination in the hepatotoxicity of cadmium. Advanced Science 10:e2203869.

Liu F, Dong W, Zhao H, *et al*., 2019. Effect of molybdenum on reproductive function of male mice treated with busulfan. Theriogenology 126:49-54.

Liu J, Li Z, Lu L, *et al*., 2022. Glyphosate damages blood-testis barrier via NOX1-triggered oxidative stress in rats: long-term exposure as a potential risk for male reproductive health. Environment International 159:107038.

Lu H, Zhang J and Xuan F, 2022. MiR-7a-5p attenuates hypoxia/reoxygenation-induced cardiomyocyte apoptosis by targeting VDAC1. Cardiovascular Toxicology 22:108-117.

Lu Y, Kan H, Wang Y, *et al*., 2018. Asiatic acid ameliorates hepatic ischemia/reperfusion injury in rats via mitochondria-targeted protective mechanism. Toxicology and Applied Pharmacology 338:214-223.

Maimaiti A, Aili A, Kuerban H, *et al*., 2018. VDAC1 mediated anticancer activity of gallic acid in human lung adenocarcinoma A549 cells. Anti-Cancer Agents in Medicinal Chemistry 18:255-262.

Miao Z, Shi X, *et al*., 2022. The antagonistic effect of selenium on lead-induced apoptosis and necroptosis via P38/JNK/ERK pathway in chicken kidney. Ecotoxicology and Environmental Safety 231:113176.

Palikaras K, Lionaki E and Tavernarakis N, 2015. Balancing mitochondrial biogenesis and mitophagy to maintain energy metabolism homeostasis. Cell Death and Differentiation 22:1399-1401.

Park E, Kim S, Song S, *et al*., 2021. Environmental exposure to cadmium and risk of thyroid cancer from national industrial complex areas: a population-based cohort study. Chemosphere 268:128819.

Shoshan-Barmatz V, Nahon-Crystal E, Shteinfer-Kuzmine A, *et al*., 2018. VDAC1, mitochondrial dysfunction, and Alzheimer's disease. Pharmacological Research 131:87-101.

Shoshan-Barmatz V, Shteinfer-Kuzmine A, Verma A. 2020. VDAC1 at the intersection of cell metabolism, apoptosis, and diseases. Biomolecules 10:1485.

Vellingiri B, Suriyanarayanan A, Abraham KS, *et al*., 2022. Influence of heavy metals in Parkinson's disease: an overview. Journal of Neurology 269:5798-5811.

Verma A, Shteinfer-Kuzmine A, Kamenetsky N, *et al*., 2023. Correction: targeting the overexpressed mitochondrial protein VDAC1 in a mouse model of Alzheimer's disease protects against mitochondrial dysfunction and mitigates brain pathology. Translational Neurodegeneration 12:2.

Wang S, Long H, Hou L, *et al*., 2023. The mitophagy pathway and its implications in human diseases. Signal Transduction and Targeted Therapy 8:304.

Wei L, Zuo Z, Yang Z, *et al*., 2022. Mitochondria damage and ferroptosis involved in Ni-induced hepatotoxicity in mice. Toxicology 466:153068.

Wu Y, Yang F, Zhou G, *et al*., 2022. Molybdenum and cadmium co-induce mitochondrial quality control disorder via FUNDC1-mediated mitophagy in sheep kidney. Frontiers in Veterinary Science 9:842259.

Xiong Z, Yang F, Dai X, *et al*., 2025. Comparative mitochondrial proteomic: PGAM5-mediated necroptosis through excessive mitophagy in sheep livers under molybdenum and cadmium co-exposure. Journal of Hazardous Materials 483:136686.

Xu S, Xiaojing L, Xinyue S, *et al*., 2021. Pig lung fibrosis is active in the subacute $CdCl_2$ exposure model and exerts cumulative toxicity through the M1/M2 imbalance. Ecotoxicology and Environmental Safety 225:112757.

Yang F, Liao J, Yu W, *et al*., 2021. Exposure to copper induces mitochondria-mediated apoptosis by inhibiting mitophagy and the PINK1/Parkin pathway in chicken (Gallus gallus) livers. Journal of Hazardous Materials 408:124888.

Zhang H, Yan J, Xie D, *et al*., 2024. Selenium restored mitophagic flux to alleviate cadmium-induced hepatotoxicity by inhibiting excessive GPER1-mediated mitophagy activation. Journal of Hazardous Materials 475:134855.

Zhong G, Wan F, Wu S, *et al*., 2021. Arsenic or/and antimony induced mitophagy and apoptosis associated with metabolic abnormalities and oxidative stress in the liver of mice. Science of the Total Environment 777:146082.